View metadata, citation and similar papers at core.ac.uk

brought to you by CORE

provided by Kyoto University Research Information Repository

KURENAI
Kyoto University Research Information Repository

KYOTO UNIVERSITY

Title	High-density excitation effect on photoluminescence in ZnO nanoparticles
Author(s)	Suzuki, Keigo; Inoguchi, Masashi; Fujita, Koji; Murai, Shunsuke; Tanaka, Katsuhisa; Tanaka, Nobuhiko; Ando, Akira; Takagi, Hiroshi
Citation	JOURNAL OF APPLIED PHYSICS (2010), 107(12)
Issue Date	2010-06
URL	http://hdl.handle.net/2433/147189
Right	Copyright 2010 American Institute of Physics. This article may be downloaded for personal use only. Any other use requires prior permission of the author and the American Institute of Physics. The following article appeared in JOURNAL OF APPLIED PHYSICS107, 124311 (2010) and may be found at http://link.aip.org/link/APPLAB/v97/i14/p142111_s1
Type	Journal Article
Textversion	publisher

Kyoto University

High-density excitation effect on photoluminescence in ZnO nanoparticles

Keigo Suzuki,[1,a)] Masashi Inoguchi,[1] Koji Fujita,[2] Shunsuke Murai,[2] Katsuhisa Tanaka,[2] Nobuhiko Tanaka,[1] Akira Ando,[1] and Hiroshi Takagi[1]
[1]*Murata Manufacturing Co. Ltd., 10-1, Higashikotari 1-chome, Nagaokakyo, Kyoto 617-8555, Japan*
[2]*Department of Material Chemistry, Graduate School of Engineering, Kyoto University, Nishikyo-ku, Kyoto 615-8510, Japan*

(Received 12 October 2009; accepted 8 April 2010; published online 22 June 2010)

In this study, photoluminescence (PL) under high excitation intensity as a function of crystalline size was systematically investigated through ZnO nanocrystalline films prepared by spin-coating a colloidal solution of ZnO nanoparticles obtained using the microemulsion method. Annealing of the films at 723, 633, and 593 K allowed us to tune the crystalline radius R. PL studies distinguished different regimes of crystalline size according to the ratio of R to the effective Bohr radius $a_B(R/a_B)$. For the sample annealed at 723 K (R/a_B=7.2), the peak of stimulated emission due to the exciton-exciton collisions appeared on the low-energy side of the exciton emission with an increase in excitation intensity. A further increase in excitation intensity eventually resulted in the occurrence of an electron-hole plasma (EHP) accompanied by consequent band gap renormalization, which indicates that high excitation intensity provokes the dissociation of excitons. For the sample annealed at 633 K (R/a_B=4.7), the stimulated emission was observed while the transition to EHP was obscure. For the sample annealed at 593 K (R/a_B=2.1), only emissions due to the recombination of the electron-hole pair were observed, and stimulated emission did not appear even when the excitation intensity was increased. The transition from free-exciton emission to donor-bound exciton emission was observed in temperature dependence of PL only for the sample with R/a_B=7.2. The origin of annihilation of the stimulated emission with a size reduction is discussed based on nonradiative Auger recombination. © *2010 American Institute of Physics*. [doi:10.1063/1.3425783]

I. INTRODUCTION

Zinc oxide (ZnO) is a promising photonic material because of its attractive physical properties and chemical stability. Its wide gap of 3.37 eV and large exciton binding energy of 60 meV are advantageous for excitonic-related device applications such as ultraviolet (UV) emitters and lasers. Nanoparticles of ZnO are expected to bring about superior optical properties owing to their quantum confinement effects, which notably enhance the performance of optical devices. For example, the third-order nonlinear susceptibility of ZnO nanoparticles was found to be approximately 500 times larger than that of bulk ZnO.[1] The photoluminescence (PL) properties of ZnO nanoparticles is important for the development of light emitting devices. In particular, the PL under high excitation intensity is crucial to elucidate the possibility of the stimulated emission in ZnO nanoparticles. So far, Tang *et al.*[2] reported stimulated emission due to an exciton-exciton collision process in nanostructured ZnO thin films with an average grain size of approximately 55 nm. To the best of our knowledge, however, the size dependence of PL behavior under high excitation intensity has not been clarified yet for ZnO nanoparticles less than several tens nanometer in diameter.

Thus far, various methods such as gas phase processes[3–7] and wet chemical reactions[8–11] have been employed to produce ZnO nanoparticles. Recently, we succeeded in fabricating a transparent colloidal solution of ZnO nanoparticles of approximately 3 nm in diameter using the microemulsion (ME) method.[12] We also reported that ZnO nanocrystalline films with crystalline sizes ranging from several to several tens of nanometers could be obtained by direct spin-coating of the solution and subsequent appropriate annealing.[13] The nanocrystalline films showed an intense UV emission with a faint green luminescence, which was attributed to their high crystallinity and low density of lattice defects. Thus, the ME-derived films are suitable for the investigation of size dependence of PL properties under the high excitation intensity.

In the present study, PL of the ME-derived ZnO nanocrystalline films with various crystalline sizes has been examined under high-density excitation. We have investigated stimulated emissions owing to radiative recombination caused by exciton-exciton collision and electron-hole plasma (EHP) that are interactions among the excitons characteristic of high excitation intensities. Especially, dependence of the stimulated emission on nanoparticle size is discussed based on nonradiative Auger recombination.

II. EXPERIMENTAL PROCEDURE

ZnO nanocrystalline films were prepared by spin-coating ME-derived ZnO colloidal solution on a quartz glass substrate and subsequent annealing at 723, 633, and 593 K. Details of preparation methods for ME-ZnO solution and nanocrystalline films have been described elsewhere.[12,13] The

[a)]Author to whom correspondence should be addressed. Electronic mail: ksuzuki@murata.co.jp.

 © 2010 American Institute of Physics

Downloaded 16 Jun 2011 to 130.54.110.72. Redistribution subject to AIP license or copyright; see http://jap.aip.org/about/rights_and_permissions

morphology, crystal structure, and crystallinity of the obtained films were investigated using a transmission electron microscope (TEM) (Model EM-002B, Topcon, Japan). X-ray diffraction (XRD) analysis with Cu $K\alpha$ radiation was also performed to evaluate the crystallite size and internal strain (inhomogeneous and homogeneous lattice strain). The XRD line profiles were fitted by the Pawley method[14] using a pseudo-Voigt function, which is expressed by a weighted sum of Gaussian and Lorentzian functions. The full width at half maximum (FWHM) of the Lorentzian and Gaussian components in the pseudo-Voigt function was estimated for each diffraction peak. The crystalline size and inhomogeneous lattice strain were calculated from the diffraction angle (2θ) dependence of the FWHM of the Lorentzian and Gaussian components, respectively. In this calculation, we assumed that the FWHM of the Lorentzian and Gaussian components is proportional to $\sec 2\theta$ and $\tan 2\theta$, respectively. Here, it should be emphasized that the present analysis allows us to estimate the crystalline sizes and inhomogeneous strain independently. Details of the calculation procedure were described elsewhere.[15] In order to evaluate the homogeneous lattice strain originating from stress in the sample, we also carried out XRD analysis using a side inclination method.[16] The tilted angle (ψ) was varied from $-60°$ to $+60°$ at the 2θ of wurtzite (110). The homogeneous lattice strain was obtained from the slope of $2\theta-\sin^2\psi$ plotting.

The dependence of PL on the excitation intensity was investigated at room temperature using the fourth harmonic of a mode-locked Nd:yttrium aluminum garnet laser (wavelength: 266 nm=4.66 eV, repetition frequency: 10 Hz, and pulse width: 25 ps) as an excitation source. The excitation light was focused on the sample surface using a planoconvex lens to yield a spot area of approximately 5 mmϕ. The luminescence from the sample was guided into a spectrophotometer through an optical fiber and detected by liquid-nitrogen-cooled charge-coupled devices. In this experiment, the excitation intensity was varied from 6 to 1018 $\mathrm{MW/cm^2}$. A continuous-wave helium cadmium (He–Cd) laser (wavelength: 325 nm=3.82 eV and power: 10 mW) was used as an excitation source for measurements of the temperature dependence of PL. The excitation light modulated by a mechanical chopper was incident on the sample surface. The PL emission from the sample was introduced into a spectrophotometer and amplified by a photomultiplier. The signals were effectively detected by synchronizing them with the trigger signals from the mechanical chopper using a two-phase lock-in amplifier. The PL spectra were measured at 12 to 300 K.

III. RESULTS AND DISCUSSION

A. Structural analysis

Figure 1 shows TEM bright-field images, high-resolution images, and selected area diffraction (SAD) patterns of the cross sections of ZnO nanocrystalline films. The bright-field images [Figs. 1(a), 1(c), and 1(e)] indicate that the films are densely packed by nanoparticles. The grains are spherical shaped, although the ZnO crystals possess a general tendency to grow unidirectionally along the *c*-axis. The SAD

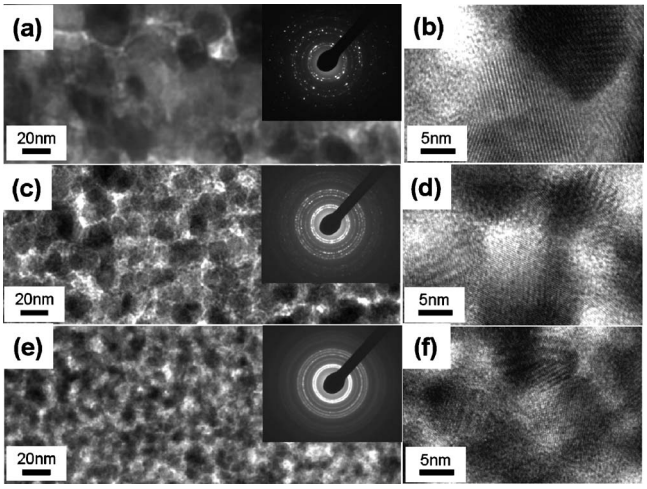

FIG. 1. (a) TEM bright-field and (b) high-resolution images of cross section of ZnO nanocrystalline film annealed at 723 K. (c) Bright-field and (d) high-resolution images of cross section of film annealed at 633 K. (e) Bright-field and (f) high-resolution images of cross section of film annealed at 593 K. The insets of the bright-field images show the SAD patterns of the corresponding samples.

patterns display clear Debye rings assigned to a single phase of the wurtzite structure. Clear lattice fringes observed in the high-resolution images [Figs. 1(b), 1(d), and 1(f)] reveal high crystallinity of the present films. As observed from the TEM bright-field and high-resolution images, the crystalline size depends on the annealing temperature. The average particle sizes estimated from TEM images by counting 100 particles are 34.3 (7.1) nm, 20.5 (3.1) nm, and 13.3 (1.8) nm for the samples annealed at 723 K, 633 K, and 593 K, respectively, where the values in parentheses are the standard deviations of size distributions.[13] The 2θ dependence of the FWHM in the XRD analysis indicates that the crystalline sizes for the samples annealed at 723 K, 633 K, and 593 K are 26.0 nm, 16.9 nm, and 7.4 nm, respectively. These crystalline sizes are almost the same as or slightly smaller than the average particle sizes estimated from TEM images. This suggests that the ZnO nanoparticles are single-crystalline in nature or consist of several crystallites. Under the assumption that the effective Bohr radius a_B=1.8 nm, as reported for bulk ZnO,[17] and taking half of the crystalline size estimated from the XRD analysis as R, we evaluated R/a_B of the samples annealed at 723 K, 633 K, and 593 K to be 7.2, 4.7, and 2.1, respectively.

The 2θ dependence of the FWHM in the XRD peaks also showed that the inhomogeneous lattice strain was approximately zero in all samples. Further, the side inclination method in XRD analysis revealed that slight homogeneous lattice strains originating in the compressive and tensile stresses were detected in the samples annealed at 633 K and 723 K, respectively, whereas no lattice strain was found in the sample annealed at 593 K. This suggests that the influence of the strain caused by annealing is faint in the present samples.

B. PL properties

Figure 2 shows the excitation intensity dependence of PL for the ZnO nanocrystalline films. Intense UV emission

Downloaded 16 Jun 2011 to 130.54.110.72. Redistribution subject to AIP license or copyright; see http://jap.aip.org/about/rights_and_permissions

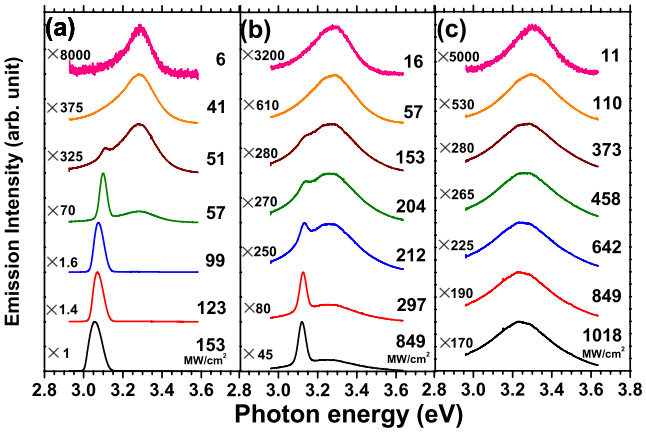

FIG. 2. (Color online) PL spectra of ZnO nanocrystalline films annealed at (a) 723, (b) 633, and (c) 593 K at various excitation intensities measured at room temperature. The magnification of the spectra is shown on the left side of each spectrum, where the magnification of the spectrum at 153 MW/cm^2 in Fig. 2(a) is set to1.

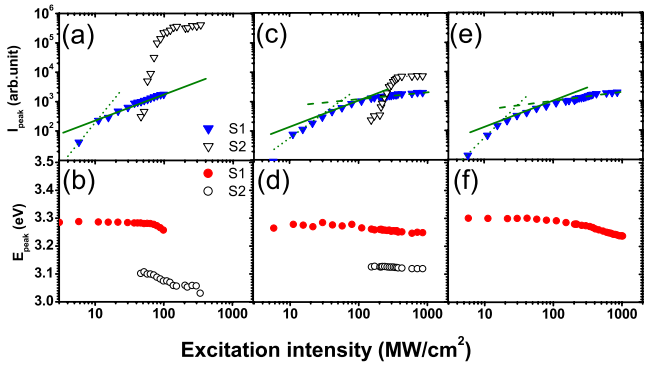

FIG. 3. (Color online) Excitation intensity dependence of (a) PL peak intensity (I_{peak}) and (b) peak energy (E_{peak}) for ZnO nanocrystalline film annealed at 723 K. Excitation intensity dependence of (c) I_{peak} and (d) E_{peak} for film annealed at 633 K. Excitation intensity dependence of (e) I_{peak} and (f) E_{peak} for film annealed at 593 K. The solid (open) triangles and circles denote I_{peak} and E_{peak} for the S1 (S2) peak, respectively. The solid lines show the linear dependence of I_{peak} (S1) on excitation intensity, while the dotted and dashed lines guide the relation at lower and higher excitation intensity regimes, respectively.

with a faint green luminescence was observed at room temperature, as reported in a previous paper.[13] For the sample annealed at 723 K [Fig. 2(a)], a UV emission peak is observed at an energy of 3.33 eV (referred to as "S1"), and is assigned to an exciton emission, when the excitation intensity is low. As the excitation intensity increases above a threshold of 51 MW/cm^2, a much narrower peak (referred to as "S2") appears at the lower-energy side of the S1 peak. The intensity of the S2 peak increases drastically with an increase in excitation intensity. The stimulated radiation due to the exciton molecular emission that occurs at temperatures below 50 K (Ref. 18) is not responsible for the S2 peak. The S2 peak seems to be a stimulated emission owing to the exciton-exciton collision process (P_2, P emission) and EHP radiative recombination (N emission) caused by high excitation intensities.[2] The PL spectra of the sample annealed at 633 K [Fig. 2(b)] also manifest the S1 and S2 peaks, whereas the S2 peak is not observed in the spectra of the sample annealed at 593 K [Fig. 2(c)]. These results will be discussed in detail below.

It may be feasible that the internal strain and defects generate nonradiative recombination pathways in the samples and hamper the observation of the stimulated emission (S2 peak). As mentioned above, no lattice strains (inhomogeneous or homogeneous strains) were detected in the sample annealed at 593 K. This indicates that annihilation of the stimulated emission in the sample annealed at 593 K is not attributable to the formation of nonradiative recombination pathways induced by internal strain. Further, the defect levels appear to be scarcely generated in the energy band gaps, since the green luminescence, which originates from impurity levels such as oxygen vacancies and interstitial zinc, is found to be faint in the present samples.[13] Hence, the effect of nonradiative recombination pathways induced by the internal strain and defects is negligible under the present annealing condition. Annealing predominantly causes the shifts in crystalline sizes, which allows us to discuss the intrinsic size effect related to changing annealing temperature.

Figure 3(a) shows the excitation intensity dependence of PL emission intensities of the S1 and S2 peaks for the sample annealed at 723 K. The intensity of the S1 peak is nearly proportional to the excitation intensity when the excitation intensity exceeds 10 MW/cm^2 (see the solid line showing a linear dependence), indicating that the PL stems from one photon process. In contrast, the intensity of the S2 peak is proportional to the sixth power of the excitation intensity and is saturated at approximately 100 MW/cm^2. Assuming that the relation between peak intensity L and excitation intensity I is $L \propto I^m$, the m values for the exciton, P_2, P, and N emissions in ZnO films were reported to be 1, 2, 8, and 5, respectively.[2] The large m values for the P and N emissions indicate the occurrence of the stimulated emission. The excitation intensity dependence of the S1 peak agrees well with the behavior of the exciton emission. The S2 peak can be ascribed to the stimulated emission due to the exciton-exciton collisions and/or EHP. The intensity of S2 peak saturates at approximately 100 MW/cm^2 and then increases depending on the relation $L \propto I^{0.42}$. This saturation implies the onset of nonradiative Auger recombination, which is a recombination process characteristic to nanocrystals and quantum wells.[19–22] The threshold intensity of the stimulated emission (S2) for the sample annealed at 723 K was estimated to be 51 MW/cm^2. This value is three orders of magnitude greater than that for nanostructured ZnO thin films prepared by molecular beam epitaxy (=24 kW/cm^2).[2] For the present ME-derived films, no laser cavity was naturally formed by the facets of hexagonal ZnO nanocrystallites arrayed in a parallel fashion.[2,23] Moreover, the crystalline sizes in the present films are much smaller than 55 nm, which was reported as an appropriate size for the occurrence of stimulated emission in ZnO.[2] These factors seem to raise the threshold intensity of the present sample. Zhang and Tang[24] reported that the threshold intensity for the stimulated emission in a ZnO film with a crystallite size of 11.2 nm was approximately 4.6 MW/cm^2. This value is one order of magnitude smaller than the threshold for the ME-derived

Downloaded 16 Jun 2011 to 130.54.110.72. Redistribution subject to AIP license or copyright; see http://jap.aip.org/about/rights_and_permissions

films, although the crystalline size reported in Ref. 24 is almost comparable to those obtained in the present study. The relation between the crystalline size and the threshold value for the stimulated emission of ZnO nanoparticles still seems to be controversial, therefore, further investigations are necessary for understanding the phenomenon thoroughly.

Figure 3(b) shows the excitation intensity dependence of PL emission energy for the S1 and S2 peaks observed in the spectra of the sample annealed at 723 K (R/a_B=7.2). The peak energy of S2 shifts from 3.11 to 3.06 eV with increasing the excitation intensity from 51 to 153 MW/cm^2. This redshift of 50 meV in the S2 peak implies that S2 in this excitation intensity region corresponds to *N* emission, since the peak energy of *N* emission is known to decrease with an increase in excitation intensity while that of *P* emission is independent of the excitation intensity.[2] For nanocrystals with R/a_B=7.2, it appears that the excitons can be easily ionized to form EHP (Mott transition) at high excitation intensities, leading to *N* emission. The strong Coulomb interaction among electrons and holes in the EHP induces band gap renormalization (BGR), which can result in the present redshift of the S2 peak. This behavior is similar to that reported in Ref. 2, indicating that the stimulated emission due to EHP is observed in ZnO nanoparticles with R/a_B=7.2. The difference between the energies of the S1 and S2 peaks [Fig. 3(b)] is estimated to be approximately 180 meV. During the exciton-exciton collision process, one of the two excitons in the $n=1$ state takes energy from the other and is converted into a higher exciton state with $n>1$, while the other decays are accompanied by a radiative photon emission. In this case, the emitted photon energy P_n is described as follows:[18]

$$P_n = E_{ex} - E_b\left(1 - \frac{1}{n^2}\right) - \frac{3}{2}kT, \quad (n = 2,3,4,\ldots,\infty), \quad (1)$$

where E_{ex}, E_b (=60 meV), and kT represent the exciton emission energy, binding energy of exciton, and thermal energy, respectively. From this equation, the energy difference between E_{ex} and *P* that corresponds to the case $n=\infty$, is calculated to be 98.7 meV at room temperature. This value is smaller by approximately 80 meV than the energy difference between the S1 and S2 peaks observed experimentally. The redshift of the S2 peak from the *P* emission peak implies that the direct transition from exciton emission to *N* emission occurs under high excitation intensities at room temperature. At high excitation intensities, the excitons in the ZnO nanoparticles with R/a_B=7.2 are dissociated to form the EHP, leading to the appearance of the *N* emission.

For the sample annealed at 633 K (R/a_B=4.7), S2 with a peak energy of 3.13 eV emerges at the excitation intensity of 153 MW/cm^2 in addition to S1 with a peak energy of 3.27 eV [Fig. 2(b)]. The threshold excitation intensity for the appearance of S2 peak is found to be larger by approximately 100 MW/cm^2 than that for the sample annealed at 723 K. Figure 3(c) demonstrates that the intensity of the S1 peak is proportional to the excitation intensity in the excitation energy range of 30–100 MW/cm^2 (see the solid line), while further increment in excitation intensity results in the saturation of peak intensity (dashed line). The intensity of the S2 peak increases with the 3.4th power of the excitation intensity and eventually saturates at 424 MW/cm^2. This *m* value (3.4) indicates the occurrence of a stimulated emission. The saturation of S2 peak intensity above 424 MW/cm^2 is again attributable to the nonradiative Auger recombination. The intensity of S2 peak above 424 MW/cm^2 depends only weakly on the excitation intensity ($L \propto I^{0.07}$). This small *m* value implies that a carrier reduction process, e.g., free-carrier absorption, occurs under the extremely high-density excitation in addition to the nonradiative Auger recombination.[20] Figure 3(d) reveals that the peak energy remains almost constant at 3.12 eV, i.e., BGR is not observed clearly. This implies that the EHP is not formed in the sample annealed at 633 K (R/a_B=4.7), in spite of the high excitation intensity.

For the sample annealed at 593 K (R/a_B=2.1), the intensity of S1 peak is nearly proportional to the excitation intensity at low excitation intensities, eventually deviating from the linear relation when the excitation intensity reaches ~60 MW/cm^2 [Fig. 3(e)]. This indicates that the nonradiative Auger recombination process appears at a lower excitation intensity compared to the samples annealed at 723 and 633 K. The FWHM of S1 emission peak increases from 0.14 to 0.20 eV [Fig. 2(c)], accompanied by a shift of the peak from 3.30 to 3.24 eV [Fig. 3(f)] when the excitation intensity is increased from 11 to 1018 MW/cm^2. Line broadening of the exciton emission has been reported for CdS nanoparticles with a size of 17 nm (R/a_B=3.7).[25] Although the stimulated emission by exciton-exciton collision was not observed in the CdS nanoparticles, this line broadening was attributable to the Mott transition and BGR. The similar broadening observed here implies that the Mott transition to the EHP occurs to some extent in the sample annealed at 593 K when the excitation intensity is high. However, stimulated emission is not clearly observed in this sample even though the excitation intensity is increased to 1018 MW/cm^2, probably due to the nonradiative Auger recombination. The probability of Auger recombination can increase with a decrease in crystalline size because in a nanosized particle, the momentum conservation law vanishes and only the energy conservation is required for the occurrence of Auger recombination.[19] Also, it has been reported that the Auger decay time τ approximately shows a cubic dependence on *R*, that is, $\tau \propto R^3$,[21] which indicates that the Auger recombination rate is rapidly enhanced by a size reduction. In order to check the size effect on stimulated emission, we also carried out PL measurements for ZnO nanocrystalline films in the range of $1.4 < R/a_B < 2.1$; however, no stimulated emission was observed even at high-excitation intensity (data not shown). Consequently, it is highly probable that the enhancement of the nonradiative Auger recombination rate by the size reduction is responsible for the absence of stimulated emission.

Figure 4 shows the temperature dependence of PL for the ZnO nanocrystalline films. It is found that the signal-to-noise ratio of the PL emission is lower for the sample annealed at 723 K [Fig. 4(a)] than for those annealed at 633 and 593 K. This behavior stems from a decrease in UV emission intensity with increasing annealing temperature. For the sample annealed at 723 K, the free-exciton emission (represented by open circles) is found to be dominant at tempera-

Downloaded 16 Jun 2011 to 130.54.110.72. Redistribution subject to AIP license or copyright; see http://jap.aip.org/about/rights_and_permissions

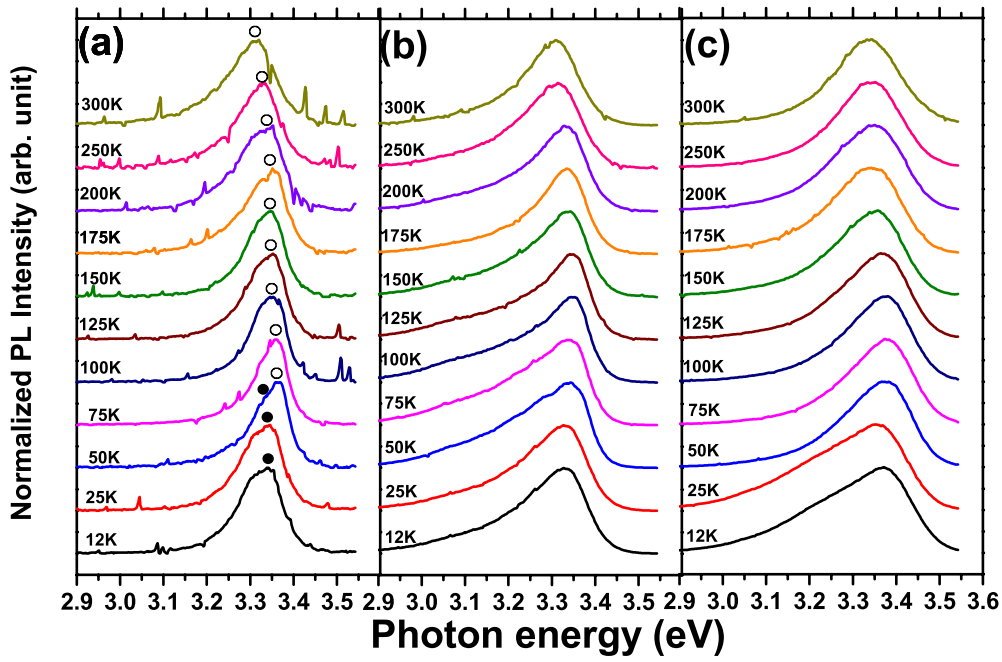

FIG. 4. (Color online) (a) PL spectra of ZnO nanocrystalline films annealed at (a) 723, (b) 633, and (c) 593 K measured at various temperatures. The open and solid circles represent the peaks of free-exciton emission and bound-exciton emission, respectively.

tures higher than 75 K. Below 50 K, however, a new peak appears at several tens of millielectron volts lower than the free-exciton peak (represented by solid circles), which eventually becomes dominant at temperatures lower than 25 K. This peak can be assigned to the bound-exciton emission in ZnO, which is a state of free excitons bound to donor centers, and appears at lower temperatures.[2] This result indicates that free excitons exist at room temperature in this sample. The peaks of UV emission for the samples annealed at 633 K [Fig. 4(b)] and 593 K [Fig. 4(c)] are broader than those of the sample annealed at 723 K. These peaks are also found to shift to the higher-energy side when the temperature is lowered. However, the peak resulting from bound-exciton emission is not obvious at low temperatures below 50 K. The disappearance of the free-exciton emission for the samples of R/a_B=4.7, and 2.1 implies the occurrence of exciton confinement by a size reduction. It is known that the localization of carrier wave function in the quantum well enhances the Auger recombination rate.[20] In a similar manner, the size reduction in nanoparticles may cause three-dimensional localization of carrier wave function. For the sample of R/a_B =2.1, it appears that the carrier localization enhances the Auger recombination rate and results in annihilation of the stimulated emission even at high excitation intensity.

IV. CONCLUSION

In this study, PL under high excitation intensity as a function of crystalline size around R/a_B=4 was systematically investigated through ME-derived ZnO nanocrystalline films. For the sample with R/a_B=7.2, the peak of the stimulated emission emerges at the low-energy side of exciton emission when the excitation intensity is above 51 MW/cm^2. For the sample with R/a_B=4.7, the transition to the EHP is not obvious, while the stimulated emission is observed at an excitation intensity above 153 MW/cm^2. For the sample with R/a_B=2.1, the stimulated emission does not appear, even though the excitation intensity is set to 1018 MW/cm^2. This could originate from the nonradiative Auger recombination process that is accelerated by a reduction in particle size. In the temperature dependence of PL, the transition from the free-exciton emission to the donor-bound exciton emission is found at 50 K in the sample with R/a_B=7.2, while such transition is not clearly found in the samples with R/a_B=4.7 and 2.1. This annihilation of free-exciton emission suggests the localization of carrier wave function, which can be one of the origins for the enhancement of nonradiative Auger recombination with the size reduction. We expect that our results provide fruitful information about the production of nanocrystalline-ZnO-based optical devices using the quantum confinement effect, such as light-emitting devices, quantum dot lasers, and nonlinear optical devices.

Note added in proof. After this paper was submitted, PL of sol-gel derived ZnO powder under high excitation intensity at low temperatures was reported by Chia *et al.*.[26] In their study, the particle size is around 30 nm (R/a_B=8.3), which is larger than that used in our study.

ACKNOWLEDGMENTS

We express our sincere gratitude to Mr. Y. Hayase, Mr. K. Akiyama, and Ms. A. Nagahara (Murata Manufacturing Co., Ltd.) for technical assistance in XRD measurements.

[1] L. Guo, S. Yang, C. Yang, P. Yu, J. Wang, W. Ge, and G. K. L. Wong, Appl. Phys. Lett. **76**, 2901 (2000).
[2] Z. K. Tang, M. Kawasaki, A. Ohtomo, H. Koinuma, and Y. Segawa, J. Cryst. Growth **287**, 169 (2006).
[3] K. Suzuki, H. Kondo, M. Inoguchi, N. Tanaka, K. Kageyama, and H. Takagi, Appl. Phys. Lett. **94**, 223103 (2009).
[4] K. K. Kim, N. Koguchi, Y. W. Ok, T. Y. Seong, and S. J. Park, Appl. Phys.

Downloaded 16 Jun 2011 to 130.54.110.72. Redistribution subject to AIP license or copyright; see http://jap.aip.org/about/rights_and_permissions

Lett. **84**, 3810 (2004).
[5]M. Ueda, S. W. Kim, S. Fujita, and S. Fujita, Jpn. J. Appl. Phys., Part 2 **43**, L652 (2004).
[6]J. G. Lu, Z. Z. Ye, J. Y. Huang, L. P. Zhu, B. H. Zhao, Z. L. Wang, and S. Fujita, Appl. Phys. Lett. **88**, 063110 (2006).
[7]J. G. Lu, Z. Z. Ye, Y. Z. Zhang, Q. L. Liang, S. Fujita, and Z. L. Wang, Appl. Phys. Lett. **89**, 023122 (2006).
[8]A. Chatterjee, C. H. Shen, A. Ganguly, L. C. Chen, C. W. Hsu, J. Y. Hwang, and K. H. Chen, Chem. Phys. Lett. **391**, 278 (2004).
[9]H. J. Chang, C. Z. Lu, Y. Wang, C. S. Son, S. I. Kim, Y. H. Kim, and I. H. Choi, J. Korean Phys. Soc. **45**, 959 (2004).
[10]H. K. Yadav, K. Sreenivas, V. Gupta, S. P. Singh, and R. S. Katiyar, J. Mater. Res. **22**, 2404 (2007).
[11]S. Mahamuni, K. Borgohain, B. S. Bendre, V. J. Leppert, and S. H. Risbud, J. Appl. Phys. **85**, 2861 (1999).
[12]M. Inoguchi, K. Suzuki, K. Kageyama, H. Takagi, and Y. Sakabe, J. Am. Ceram. Soc. **91**, 3850 (2008).
[13]M. Inoguchi, K. Suzuki, N. Tanaka, K. Kageyama, and H. Takagi, J. Mater. Res. **24**, 2243 (2009).
[14]G. S. Pawley, J. Appl. Crystallogr. **14**, 357 (1981).
[15]A. C. Larson and R. B. Von Dreele, "General Structure Analysis System (GSAS)," Los Alamos National Laboratory Report No. LAUR 86–748, 2000 (unpublished).
[16]E. Macherauch and P. Mueller, Z. Angew. Phys. **13**, 305 (1961).
[17]I. Broser, R. Broser, H. Finkenrath, R. R. Galazka, H. E. Gumlich, A. Hoffmann, J. Kossut, E. Mollwo, H. Nelkowski, G. Nimtz, W. von der Osten, M. Rosenzweig, H. J. Schulz, D. Theis, and D. Tschierse, *Semiconductors: Physics of II-VI and I-VII Compounds, Semimagnetic Semiconductors*, Landolt Bornstein, New Series, edited by O. Madelung, Vol. 17 (Springer-Verlag, Berlin, 1982).
[18]S. W. Koch, H. Haug, G. Schmieder, W. Bohnert, and C. Klingshirn, Phys. Status Solidi B **89**, 431 (1978).
[19]*Optical Properties of Semiconductor Nanocrystals*, edited by S. V. Gaponenko (Cambridge University Press, Cambridge, 1998), p. 143.
[20]T. Tayagaki, S. Fukatsu, and Y. Kanemitsu, Phys. Rev. B **79**, 041301 (2009).
[21]A. Ueda, T. Tayagaki, and Y. Kanemitsu, J. Phys. Soc. Jpn. **78**, 083706 (2009).
[22]V. I. Klimov, S. A. Ivanov, J. Nanda, M. Achermann, I. Bezel, J. A. McGuire, and A. Piryatinski, Nature (London) **447**, 441 (2007).
[23]Z. K. Tang, G. K. L. Wong, P. Yu, M. Kawasaki, A. Ohtomo, H. Koinuma, and Y. Segawa, Appl. Phys. Lett. **72**, 3270 (1998).
[24]L. Z. Zhang and G. Q. Tang, Opt. Mater. **27**, 217 (2004).
[25]Y. Kanemitsu, T. J. Inagaki, M. Ando, K. Matsuda, T. Saiki, and C. W. White, Appl. Phys. Lett. **81**, 141 (2002).
[26]C. H. Chia, Y. J. Lai, T. C. Han, J. W. Chiou, Y. M. Hu, and W. C. Chou, Appl. Phys. Lett. **96**, 081903 (2010).

Downloaded 16 Jun 2011 to 130.54.110.72. Redistribution subject to AIP license or copyright; see http://jap.aip.org/about/rights_and_permissions